Journal of Marine Science and Technology

Volume 27 | Issue 2 Article 2

EXPERIMENTAL STUDY OF SCOUR AROUND MONOPILE AND JACKET-TYPE OFFSHORE WIND TURBINE FOUNDATIONS

Hsin-Hung Chen
Department of Hydraulic and Ocean Engineering, National Cheng Kung University, Tainan, Taiwan, R.O.C.

Journal of Marine Science and Technology, Vol. 27, No. 2, pp. 91-100 (2019)
DOI: 10.6119/JMST.201904_27(2).0002

EXPERIMENTAL STUDY OF SCOUR AROUND MONOPILE AND JACKET-TYPE OFFSHORE WIND TURBINE FOUNDATIONS

Hsin-Hung Chen, Ray-Yeng Yang, Shih-Chun Hsiao, and Hwung-Hweng Hwung

Key words: offshore wind turbine, monopile, jacket-type, the maximum scour depth.

ABSTRACT

Wind turbines platforms and pillars on offshore wind farms are negatively affected by wave and current action. In Taiwan, the water depth of most planned wind turbine foundations is more than 15 m. At this water depth, scour around offshore wind turbine foundations is mainly subject to the ocean current, which causes damage or collapse of foundations. Therefore, this study focused on the influence of ocean current on the monopile and jacket-type foundations of offshore wind turbines. Hydraulic model experiments were conducted to investigate the maximum scour depth and range around pillars in these foundations. Under the effects of current, the relationships between the dimensionless maximum scour depth corresponding to the Froude number (F_r) and Reynolds number (R_e) were calculated and compared with the experimental results. Then, a relationship between the Reynolds number (R_e) and the relative scour water depth ($d_{s,max}/h$) could be obtained as a regression curve. In addition, this regression curve could be used to estimate the maximum scour depth around the monopile and jacket-type foundations under different current velocity (U), water depth (h) and pile diameter (D) conditions. The findings are valuable as a design reference for offshore wind turbine foundations.

I. INTRODUCTION

Taiwan is an island country that has extremely low fossil fuel resources; 98% of Taiwan's energy supply is derived from foreign imports. However, Taiwan's climate is characterized by prevalent monsoons, indicating that Taiwan has excellent wind resources. The winds over the western coast are especially well suited for onshore and offshore wind power generation. Wind power generation can reduce not only Taiwan's overdependence on energy imports but also the risk of electricity crises in Taiwan. In addition, wind energy is nearly pollution free and thus beneficial to sustainable development. Taiwan's government actively promotes the utilization of renewable energy, aiming at strengthening energy autonomy and responding to climate change. The government aims for renewable energy to represent 20% of total power generation by 2025 and has set a target of 5.5 GW for offshore wind capacity. This target suggests that the development of offshore wind power generation is an urgent matter. Offshore power generation has great potential for Taiwan. To effectively utilize wind resources, offshore wind turbine bases must be selected based on considerations of Taiwan's special typhoon- and earthquake-prone environment. Suitable bases may be used to establish offshore wind farms and offshore wind energy industries.

At present, offshore wind turbines in Taiwan are installed underwater at depths of 10 to 50 m. Six types of offshore wind turbine foundations are available worldwide: (1) monopile, (2) tripile, (3) tripod, (4) jacket type, (5) gravity base, and (6) floating. The choice and size of the foundation depend on the water depth, current, and seabed. Monopile is the mainstream type of underwater foundation used in Europe and is mostly applied in areas where the water depth is less than 20 m. The jacket-type foundation involves a more complicate truss structure; therefore, its manufacture is labor intensive and relatively costly. However, the jacket-type foundation is relatively stable and is suitable for use in soft soil ground and active seismic zones. Taiwan is located in the Pacific Ring of Fire and is hit by typhoons almost every summer; thus, both earthquake- and typhoon-related factors must be considered while selecting the wind turbine foundation type for the development of wind farms. It is understood that marine structures in the ocean are always subjected to wave and current action, so scour, which is sea-floor erosion caused by strong tidal currents resulting in the removal of inshore sediments and formation of deep holes and channels, will be induced around the foundation of ocean structures. These phenomena may result in damage to or collapse of an offshore wind turbine foundation. In order to understand the mechanism of scour around the offshore wind turbine foundation, elaborate hydraulic model tests of monopile and jacket-type foundations are con-

Paper submitted 10/16/18; revised 01/02/19; accepted 01/30/19. *Author for correspondence: Hwung-Hweng Hwung (e-mail: hhhwung@mail.ncku.edu.tw). Department of Hydraulic and Ocean Engineering, National Cheng Kung University, Tainan, Taiwan, R.O.C.*

ducted to investigate the evolution of scour scope and depth around such foundations.

In practice, engineered ocean structures will change the dynamic sediment conditions of the surrounding environment as well as the original current and wave fields. Scour around structures refers to the lowering of the surrounding bare seabed. This phenomenon may result from local acceleration (or deceleration) of the current velocity close to the seabed or increased local sediment transport due to turbulent flow (or vortex). Once a scour hole is formed, a flow separation phenomenon occurs and a mixed layer develops on the front edge of the hole that results in greater turbulence intensity and further scouring. Raudkivi and Ettema (1983) identified three types of scour based on flow speed: general, contraction, and local. General scour occurs regardless of whether a physical structure is present. Contraction scour is caused by shrinking waterways. Finally, local scour is caused by changes of the flow pattern caused by the structures. The experimental results of Raudkivi and Ettema (1983) revealed that the factors influencing the development and the equilibrium depth of local scour around cylindrical piers include flow velocity, flow depth, pile diameter, and the particle size of the bed sediment. Breusers et al. (1977) examined the case of a single pile located in a uniform seabed and determined that the depth of scour (d_s) near the pile was related to the diameter of the pile (D). Moreover, research findings have also indicated that gradation of a seabed significantly influences scour depth, because coarse grains in the upper part of the scour hole exhibit a protective effect. In addition, scour around a vertical pile is associated with waves; the horseshoe vortices induced by waves are less pronounced when the wave boundary layer is thinner.

On the basis of test results for a vertical cylinder, Sumer et al. (1992, 1993) summarized the relationship between the maximum scour depth ($d_{s,max}$) and pile diameter (D) for three types of pile geometry (circular piles and square piles with 90° and 45° orientations). Hotta and Mauri (1976) studied the scour depths of piles in the surf zone of Ajigaura beach, Japan. The researchers determined that the maximum scour depth $d_{s,max}/D$ was 1-1.5 and that the maximum scour length with respect to the pipe axis (L/D) was 7-10. den Boon et al. (2004) studied the occurrence and prevention of scour holes around the monopile foundations of offshore wind turbines in a physical model test. It was found that a scour hole of 6 to 7.4 m depth developed around a 4.2 m diameter monopile, depending on current and wave conditions. Zhao et al. (2010) experimentally and numerically investigated local scour around a submerged vertical circular cylinder in the presence of steady currents. Stahlmann and Schlurmann (2012) studied the scour of tripod foundations using both large-scale physical experiments and a numerical simulation. Their experimental results indicated that scour occurs not only around the wind turbine foundation but also at the abutment. In this study, the evolution of scour depth and scope around monopile and jacket-type foundations under different current velocities was investigated. Furthermore, the relationships between the dimensionless maximum scour depth and the test duration and the dynamic parameters were also obtained.

II. HYDRAULIC MODEL EXPERIMENT

In this study, a movable-bed experimental design was used to realistically simulate either scour or sediment behavior caused by a two-phase current around monopile and jacket-type foundations. Because of the characteristics of seabed sediments, different movement states and research purposes, three-dimensional movable-bed model tests have been conducted in hydraulic experiments. On the basis of Kamphuis' studies, Oumeraci (1984) proposed four principal similarity criteria for sediment transport in a movable-bed test: the grain Reynolds number, Shields parameters related to sediment initiation, relative density of soil grains (ρ_s/ρ_w), and relative length scale of a/D_{50} (a = wave amplitude and D_{50} = grain diameter at 50 wt%). The aforementioned similarity criteria cannot be met simultaneously in the test model. Therefore, possible scale effects must be taken into account when neglecting a criterion. For example, in the case of the scale effects of the grain Reynolds number, light materials are preferable for a drift sand transport test model to maintain similar values to those of a prototype and reduce the scale effects. As to the scale effects of the Shields parameters for initiation of motion, a dissimilarity between the grains applied in the test model and those in the prototype results in dissimilar sediment initiation and may exaggerate the time scale of sediment transportation. Oumeraci (1984) reported that different Shields parameters will produce relatively different sand ripple patterns which will change the seabed friction and the attenuation of incident waves. However, Dean and Dalrymple (1985) argued that the Shields parameter similarity is not critical to a determination of beach terrain changes, because sediment movement is disturbed by wave breaking rather than by shear stress. Dean and Dalrymple concluded that the speed of sediment subsidence can serve as an approximation of the Shields parameter. In terms of the scale effects of relative sediment density, lighter sand materials in a model causes the sands to prematurely move into a suspended condition, increasing the sediment transport rate and reducing the subsiding volume within the broken zone. By contrast, heavier sand materials inhibit the movement of model sands and increase the subsiding volume within the broken zone. Finally, the relative length scale effects between the wave amplitude and the sediment particle, and the scale dissimilarity between the relative density ρ_s/ρ_w and the relative length a/D_{50} result from the lighter sand used in movable-bed experiments. Therefore, the density and diameter of sand grains must also to be selected carefully in such experiments.

Considering the possible scale effects discussed above, most studies have indicated that regardless of the kind of model criteria, a relatively large model scale should be used to reduce scale effects. If conditions permit, a series of scale tests can be conducted preliminarily. For the sake of rigor, the results of these tests should be compared with on-site prototype data, and the parameters of the model scale should be adjusted accordingly. In this study a model scale of 1/36 was used based on considerations of factor constraints, including the Shields parameters, power conditions, the scope of the experiment, experi-

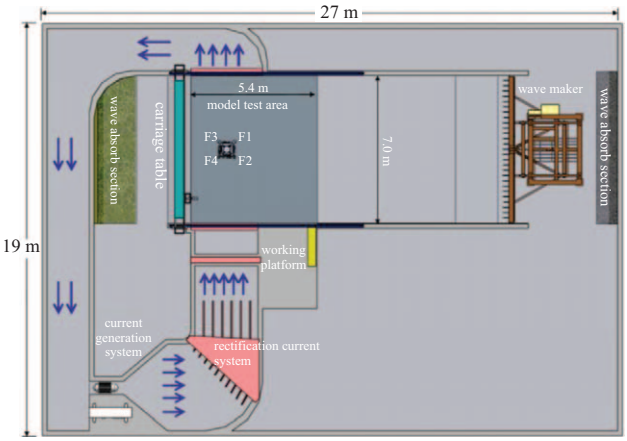

Fig. 1. Diagram of the layout of the hydraulic model test.

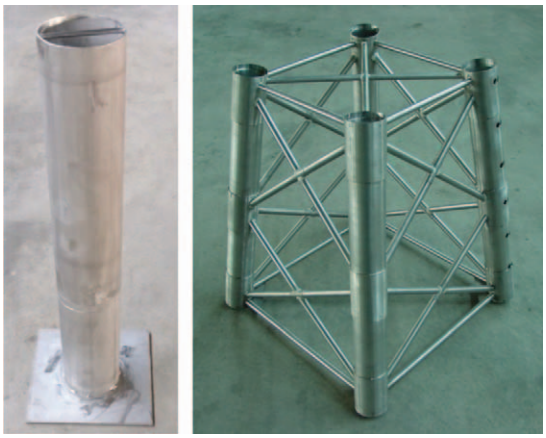

(a) monopile (b) jacket-type

Fig. 2. Models of monopile and jacket-type foundations.

mental equipment, the laying thickness of the seabed, and the size of the test site.

The hydraulic model experiment was performed in a wind-wave-current basin (WWCB) at National Cheng Kung University's Tainan Hydraulics Laboratory. The WWCB is 27 m in length, 19 m in width, and 1 m in depth and can simultaneously generate wind, waves, and current. The current-generation system consisted of a set of axial-flow pumps that could generate both positive and negative flows. The pump speed was as high as 50 Hz, providing a maximum flow of approximately 0.4 CMS. A current-rectification apparatus comprising a flow-guiding panel and a honeycomb structure consisting of straws with lengths of 20 cm and diameters of 0.8 cm was used to ensure that the various flows were stable and of similar quality (Chen et al., 2014). Adjustable diversion facilities were established in the inflow port in front of the test section and in the outflow port in back of the test section and were used to adjust the inflow angle. Fig. 1 provides a layout diagram of the hydraulic model test. In the model test area, a movable-bed (coal bed) test area 3.4 m in length, 7 m in width, and 0.35 m in height was laid. The left and right sides of the movable-bed test area were the circulation channels of the flow, and the flow was created using the axial-flow motor. The flow during the test process was stabilized and rectified using a deflector and honeycomb rectification facilities, respectively. The base model was erected near the center of the movable-bed test area.

Tracks and trolleys were erected in the test area, and acoustic doppler velocimeters (NORTEK Vectrino Plus) and an ultrasonic bottom profiler (SeaTek, 5 MHz Ultrasonic Ranging System) were mounted on the trolley. A set of acoustic doppler velocimeters was mounted on the up-current side of the frontal foundation to measure the current rate. The sensor of the acoustic doppler velocimeter was positioned 5 cm from the bottom of the bed to measure the velocity near the bed. The measurements of topographic changes were mainly focused on scour areas around the observation tower. In total, 48 measurement lines were arranged in front of and behind the observation tower. The measured line spacing was 2 cm; the measured point spacing was 2 cm; and each measurement line involved 56 measurement points. The total measurement range encompassed 2,688 measurement points.

Monopile and jacket-type foundations were chosen for the hydraulic model movable-bed experiment in this study because these foundation types are frequently used in the international offshore wind field and are applicable to the western ocean of Taiwan. Fig. 2 presents models of monopile and jacket-type foundations. The monopile foundations at the research site have diameters of 4.2 and 6 m, and the jacket-type foundation has a pile diameter of 2.08 m. As described, the scale of the hydraulic model test was 1/36; therefore, the modeled monopile foundations had diameters of 0.117 and 0.167 m, and the model of the jacket-type foundation had a pile diameter of 0.058 m.

We took into consideration that when the water depth exceeds 15 m in actual sea areas, the scour effect around structures caused by a monsoon wave is lower than that caused by the current. If the wave height is 1.0 m, and the period is 5 sec of monsoon wave, the bottom velocity is approximately 0.11 m/sec. KC = 0.09 for a 6m monopile diameter, so the KC value is relatively small. Therefore, it is mainly based on current. (KC is the Keulegan-Carpenter number; KC = UT/D, where U is the flow velocity near the bed; T is the wave period, and D is the diameter of the pile.) In this study, the scour of the structure is initially considered based on the current. Therefore, to explore current-induced scour around the wind turbine foundation, a series of scour experiments with various current velocities, water depths, and pile diameters were performed in this study. The related parameter conditions for the foundation scour experiments are listed in Table 1.

When investigating the scouring phenomenon of a seabed, external forces that cause the scouring must be understood. Additionally, thorough identification and assessment of the physical properties of bed materials are required. These properties include particle size, shape, roundness, porosity, specific gravity, water permeability, and mineral composition, among which particle size and specific gravity are particularly critical. In the scale model, the sediment movement under the scale-down of

Table 1. Related parameter conditions for the foundation scour experiment.

Test case	Diameter D (m)	Water depth h (m)	Current speed U (m/s)	F_r	R_e
MSV125	0.117 (D_1)	0.500	0.125	0.056	1.46×10^4
MSV167			0.167	0.075	1.94×10^4
MSV211			0.211	0.095	2.46×10^4
MSV250			0.250	0.113	2.92×10^4
MV125	0.167 (D_2)	0.444	0.125	0.060	2.08×10^4
MV167			0.167	0.080	2.78×10^4
MV208			0.208	0.100	3.47×10^4
MV250			0.250	0.120	4.17×10^4
JV083	0.058 (D_3)	0.444	0.083	0.040	4.81×10^3
JV167			0.167	0.080	9.63×10^3
JV250			0.250	0.120	1.44×10^4

* D_1 and D_2 represent diameters of monopile foundations; D_3 denotes the diameter of the jacket-type foundation; F_r is the Froude number, and R_e represents the Reynolds number.

Table 2. Principal properties of coal ash.

Specific gravity	2.05
Median particle diameter (mm)	0.15
Repose angle (dry)	27°
Repose angle (wet)	69°
Sediment settling velocity (cm/sec)	1.19
Saturation (%)	22.5
Porosity ratio	2.54
Porosity (%)	71.6

hydrodynamics was similar to that of the sand movement. Selection of appropriate sediment materials is key to the success of drift and scour experiments. Therefore, the principal properties of coal ash were analyzed, and then it was applied as the experimental sediment material. The principal properties examined included specific gravity, particle size, repose angle, sediment settling velocity, saturation, porosity ratio, and porosity, for which the results are denoted in Table 2.

III. EXPERIMENTAL RESULTS

1. Monopile Foundation

In the scour experiments of the monopile offshore wind turbine foundations, operations of 10 to 60 minutes depended on the magnitude of the velocities and possible changes in topography, and currents were stopped at intervals so that the topography could be measured. When the change in the bed scour depth reached equilibrium, the current maker was stopped, and the final profile was measured. Fig. 3 presents data regarding the monopile foundation ($D_1 = 0.117$ m and $D_2 = 0.167$ m), the change in the ratio (d_s/D) of the scour depth (d_s) to the monopile diameter (D), and the test durations for four current velocities.

The experimental results indicated that when the current velocity was relatively small (MSV125 and MV125), the scour rate around the monopile was relatively low. When the current continued for 480 minutes, the scour depth approached stability. The current-generation system stopped after activity for 600 minutes. With increases in the current velocity, the scour rate clearly increased, especially in the test of the largest current ve-

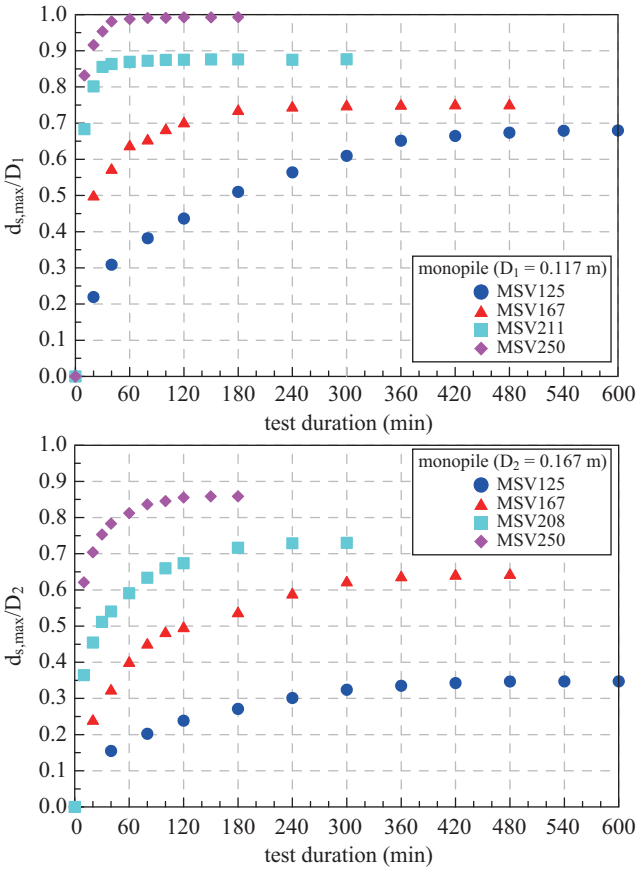

Fig. 3. Relationship between the dimensionless scour depth ($d_{s,max}/D$) and the test duration for monopile foundations under different currents.

Table 3. Maximum scour depth around the monopile foundations under various conditions.

D_1 = 0.117 m			D_2 = 0.167 m		
Test case	$d_{s,max}/D_1$	$d_{s,max}/h$	Test case	$d_{s,max}/D_2$	$d_{s,max}/h$
MSV125	0.68	0.16	MV125	0.35	0.13
MSV167	0.75	0.18	MV167	0.65	0.24
MSV211	0.88	0.20	MV208	0.73	0.27
MSV250	0.99	0.23	MV250	0.86	0.32

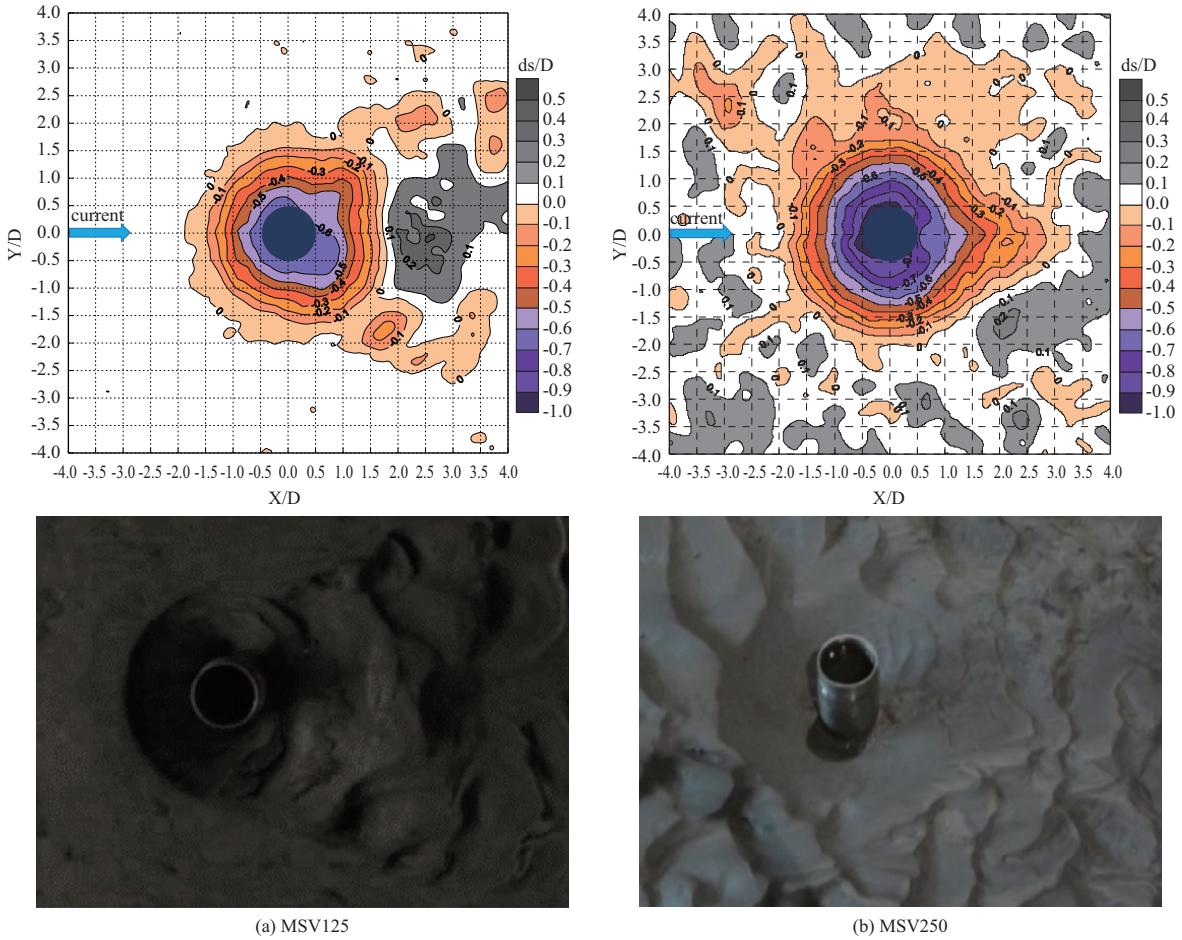

(a) MSV125 (b) MSV250

Fig. 4. Scour range and topography around the monopile foundation (D_1 = 0.117m) under various current velocities.

locity (MSV250 and MV250). The greatest change in the maximum scour depth occurred after 10 and 30 minutes of current activity. After 40 minutes of current activity, the change in the maximum scour depth slowed. The final maximum scour depth was reached after the first 60 minutes and thereafter remained stable for the cumulative test duration up to 180 minutes. For the larger monopile diameter (D_2 = 0.167 m), an increase in current velocity corresponded with an increase in the maximum scour depth. Under the current velocity of 0.25 m/s, the maximum scour depth for the D_2 monopile diameter was 0.86 D_2, and the maximum scour depth for the D_1 monopile diameter was 0.99 D_1. Table 3 indicates the ratios of the maximum scour depth ($d_{s,max}$), the diameters of the monopiles (D_1 and D_2), and the water depth (h) around the monopile foundations under currents at four velocities. One trend was the same between the two diameters: with an increase in current velocity, the dimensionless ratios of the maximum scour depth ($d_{s,max}/D$ and $d_{s,max}/h$) also increased. However, the larger monopile diameter (D_2 = 0.167 m) exhibited a greater maximum scour depth ($d_{s,max}$) under increasing current velocities.

The terrain variations around the foundation of monopile offshore wind turbines under currents at four velocities were examined. The experimental results indicated that under a small current velocity of 0.125 m/s (MSV125 test), the scour ranges were similar for the up-current side and down-current side. The scour pits were approximately circular. The relationship based

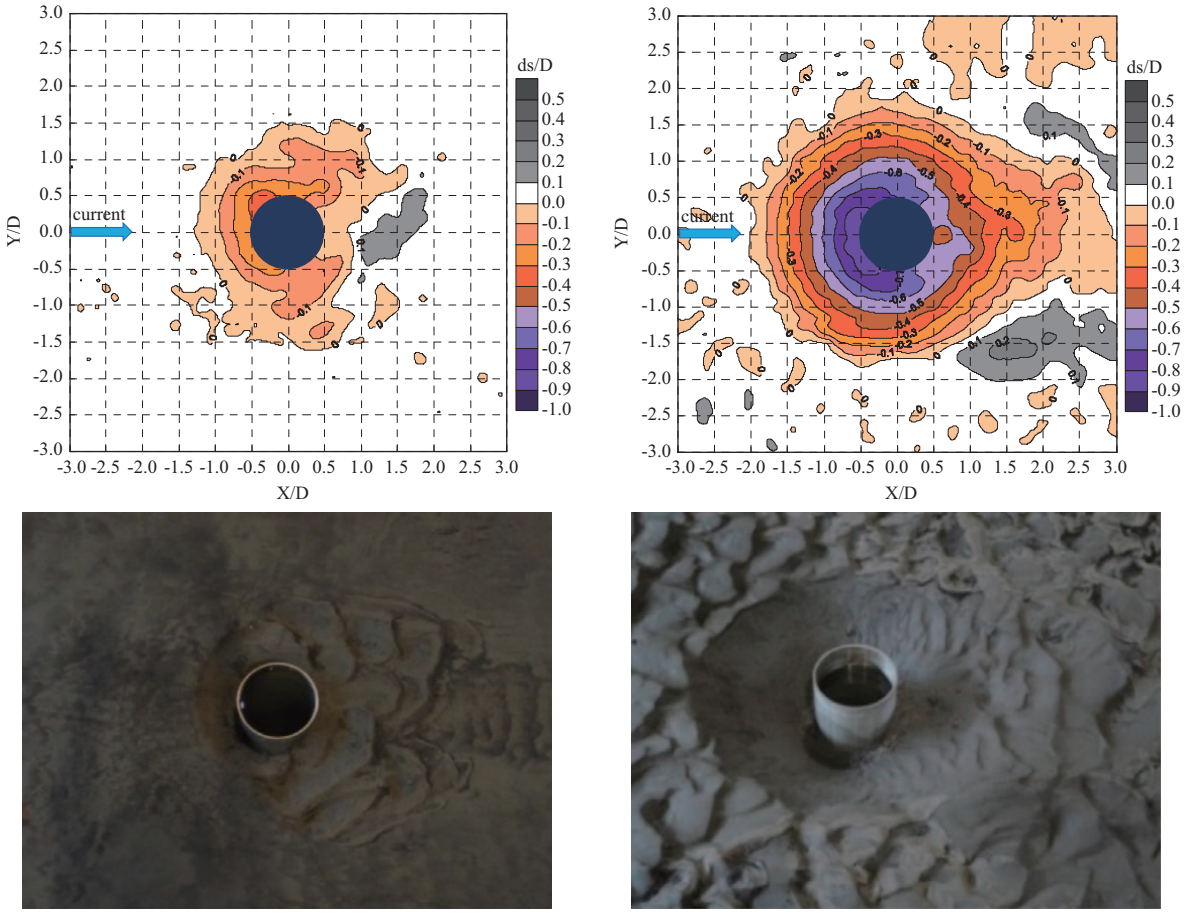

(a) MV125 (b) MV250

Fig. 5. Scour range and topography around the monopile foundation (D_2 = 0.167m) under various current velocities.

on the wake vortex between the two sides of the monopile down-current still exhibited slight scouring. Deposition was also observed behind the monopile as shown in Fig. 4(a). Under the large current velocity of 0.250 m/s (MSV250 test), a semicircle-type scour pit formed on the front side of the monopole column, and a cone-shaped scour pit formed in the rear. The scour range on the up-current side was slightly larger and that on the down-current side exhibited an expansion trend. Fig. 4(b) depicts the topography of the monopile with diameter D_1 under a current velocity of 0.250 m/s. The other two topographic changes between the smaller and larger current velocities were similar to the described phenomenon, except that the scour range varied according to the current velocity.

Fig. 5 illustrates the topography of the monopile with diameter D_2 for the current velocities 0.125 m/s (MV125 test) and 0.250 m/s (MV250 test). Under these current velocities, a semicircle-type scour pit was still observed in front of the D_2 monopile, and the range of the scour pit gradually expanded with the current velocity. The scour pit on the down-current side increased with the current velocity. The semicircle-type shape gradually transformed into a cone shape, and the entire scour area gradually expanded. The observed changes in the scour pit were similar to those observed in the tests of the D_1 diameter monopole foundation.

Overall, with increases in the current velocity, the up-current-side scour range increased for the scour pits in the case of the two sets with different pile diameters, and the scour range of the down-current side also increased. The same scour occurred regardless of the pile diameter. The maximum scour profile test results for the monopile diameters and current velocities are plotted in Fig. 6. With increases in the current velocity, the maximum scour depth of the up-current side and down-current side also increased. However, the maximum scour depth of the D_2 monopile diameter was greater than that of the pile with the smaller diameter D_1. This finding offers a reference for engineering design. Table 4 denotes the scour range of the monopile offshore wind turbine foundation at approximately the maximum scour depth and in relation to current action (the scour range is indicated by the monopile diameter D).

When the current velocity was 0.125 m/s (MSV125 test) and the maximum scour depth was reached, the scour range, which was measured from the axis center of the monopile foundation at the up-current side, was 1.9 D_1 and that of the down-current side was 1.8 D_1; the scour pit was approximately circular. When the

Table 4. Maximum scour range around the monopile foundation under various conditions.

Test Case	MSV125	MSV167	MSV211	MSV250
up-current	1.9 D_1	2.0 D_1	2.1 D_1	2.5 D_1
down-current	1.8 D_1	2.3 D_1	3.1 D_1	3.9 D_1
Test Case	MV125	MV167	MV211	MV250
up-current	1.3 D_2	1.8 D_2	1.9 D_2	2.2 D_2
down-current	1.6 D_2	2.1 D_2	2.9 D_2	3.1 D_2

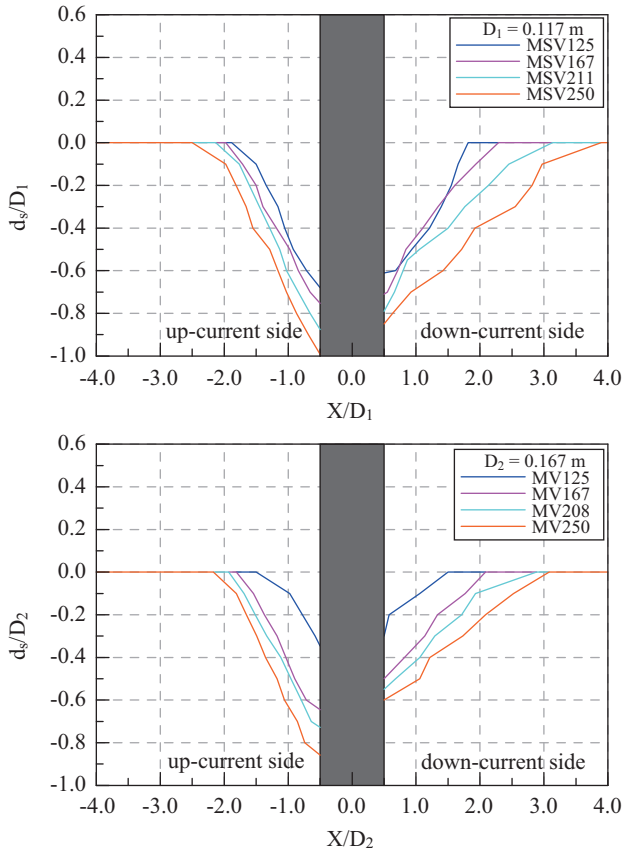

Fig. 6. Profiles of the scour pit around the monopile foundation under various currents.

current velocity was 0.167 m/s (MSV167), the scour range of the up-current side was approximately 2.0 D_1, and that of the down-current side was 2.3 D_1. The scour range exhibited a slight trend toward enlargement, and the scour range of the down-current side clearly increased. When the current velocity was 0.211 m/s (MSV211 test), the scour range of the up-current side was approximately 2.1 D_1, and that of the down-current side was 3.1 D_1. Additionally, the scour range of the down-current side exhibited a greater increase, and a cone-shaped scour pit gradually formed on this side. Finally, when the velocity reached 0.25 m/s (MSV250 test), the scour range of the up-current side was approximately 2.5 D_1, and that of the down-current side was 3.9 D_1; the scour range of the up-current side was larger, and

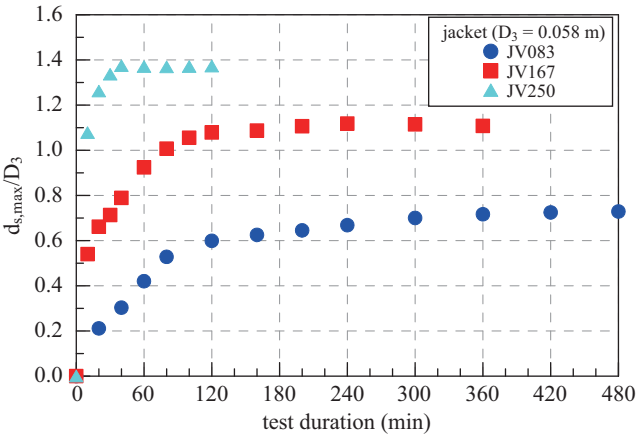

Fig. 7. The relationship between the dimensionless scour depth ($d_{s,max}/D$) and the test duration for the jacket-type foundation under various currents.

the scour range of the down-current side grew to a greater extent.

The scour range around the monopile of diameter D_2 exhibited the same trend. When the maximum velocity was 0.25 m/s (MV250 test), the scour range of the up-current side was 2.2 D_2; those of the two sides of the monopile were approximately 2.0 D_2, and that of the down-current side was 3.1 D_2. The scour pit range of the up-current side was semicircular, and that of the down-current side was cone shaped. The test results indicated that increases in current velocity around the monopile foundation correlated with the formation of scour pits with larger ranges. The scour ranges of the up-current and down-current sides also increased, and the scour range of the down-current side increased significantly. When the current velocity was 0.25 m/s, the scour range of the D_1 monopile diameter was approximately 1.3 times the 0.125 m/s current velocity, and that of the down-current side was 2.2 times the velocity. The scour range of the up-current side of the D_2 monopile diameter was approximately 1.7 times the current velocity under a velocity of 0.125 m/s velocity, and the scour range of the down-current side was 1.9 times the current velocity.

2. Jacket-Type Foundation

The layout of the scour test for the jacket-type foundation used in offshore wind farms is depicted in Fig. 1. As denoted in the figure, the piles of the jacket-type foundation were defined as follows: F_1 was the right pile on the up-current side; the left pile was F_2, and the right and left piles of the down-current side were defined as F_3 and F_4, respectively. The diameters of the four piles (D_3) were all 0.058 m.

In the jacket-type foundation scouring test, the maximum scour was reached at a velocity of 0.083 m/s after 480 minutes of current action. Under the large current velocities of 0.167 m/s and 0.25 m/s, the current action had to be paused every 10 minutes so that topographic measurements could be obtained, and 360 and 120 minutes were required, respectively, to achieve the maximum scour. Fig. 7 illustrates the relationship between the dimensionless scour depth ($d_{s,max}/D_3$) of the single pile (F_2)

Table 5. Maximum scour range around the jacket-type foundation under various conditions.

Test case	$d_{s,max}/D_3$				$d_{s,max}/h$			
	F_1	F_2	F_3	F_4	F_1	F_2	F_3	F_4
JV083	0.66	0.73	0.35	0.40	0.09	0.09	0.05	0.05
JV167	1.12	1.11	0.61	0.76	0.15	0.14	0.08	0.10
JV250	1.24	1.37	0.70	0.62	0.16	0.18	0.09	0.08

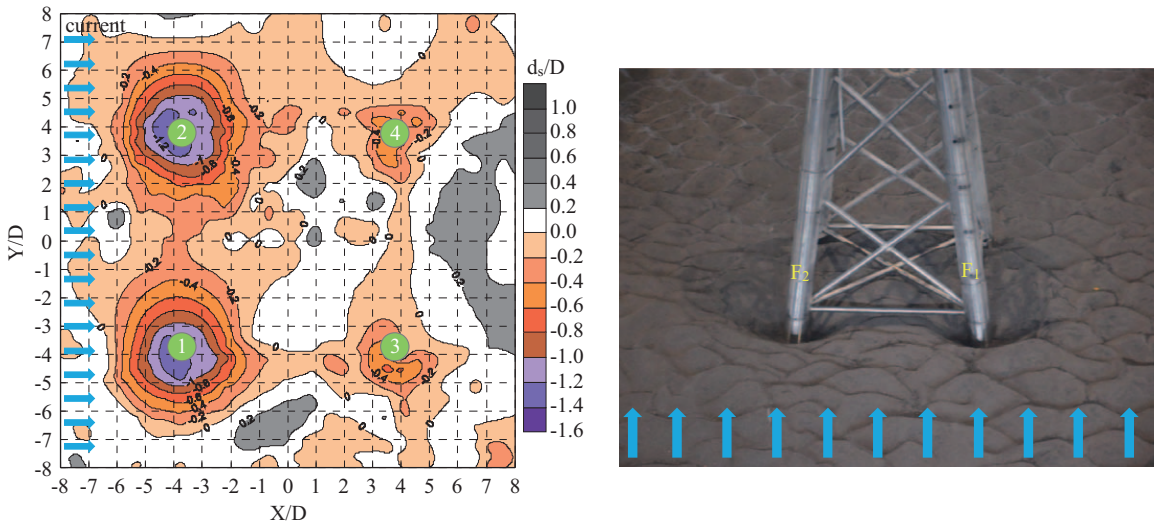

Fig. 8. Scour range and topography around the jacket-type foundation (D_3 = 0.058 m) under a current velocity of 0.25 m/s (JV250).

and the test duration for the jacket-type foundation under three current velocities. The results revealed that the change in scour depth was more pronounced before 120 minutes under a current velocity of 0.083 m/s; the change in scour depth after 120 minutes was slow, and the scour depth was nearly stable after 300 minutes of current action. The maximum scour depth was approximately 0.73 D_3 after 480 minutes of current action. At a current velocity of 0.167 m/s, the scour depth changed significantly between 10 and- 60 minutes. After the 80-minute point of current action had been reached, the change in scour depth slowed. In the period after 120 minutes of continuous effect, the scour depth changed little and tended toward stability. The maximum scour depth was approximately 1.11 D_3 when the current test duration had reached 360 minutes. When the current velocity was 0.250 m/s, the maximum scour depth changed significantly within the first 10-30 minutes of current action. After 30 minutes, the maximum scour depth change slowed, and the scour depth approached its maximum after 40 minutes. The maximum scour depth was approximately 1.37 D_3 after a continuous current had been applied for 120 minutes. The maximum scour depths around the other piles of the jacket-type foundation for the three current velocities exhibited the same trend.

In the experiment on application of currents to the jacket-type foundation, scour occurred around the F_1 and F_2 piles on the up-current side, whereas scour around the F_3 and F_4 piles on the down-current side was less obvious. Scour was affected by the shadowing effect and changes in the current field. In the JV250 test, the maximum scour depth occurred on the up-current side of the F_2 pile and was 1.37 D_3, and the scour around the F_1 pile on the up-current side was 1.24 D_3. The scour around the F_3 and F_4 piles on the down-current side was not significant, and the scour depth and range were small. However, deposition occurred behind the jacket-type foundation as a result of the shielding of the foundation structure. Fig. 8 presents the scour range and topography around the jacket-type foundation (D_3 = 0.058m) under a current velocity of 0.25 m/s (JV250). The test results revealed that the scour of the greatest depth was formed by the F_1 and F_2 piles on the up-current side. Three current velocities (0.083, 0.167, and 0.25 m/s) were tested; under higher current velocities, the scour depths around the four foundation piles were larger. The maximum scour depths around the jacket-type foundation piles were 0.73, 1.12, and 1.37 D_3, respectively, for the aforementioned currents. Table 5 lists the ratios ($d_{s,max}/D_3$ and $d_{s,max}/h$) of the maximum scour depth to the pile diameter as well as the water depth after the current test of the jacket-type foundation.

Overall, for the jacket-type foundation under three current velocities, the scour range of the foundation pile (F_1 and F_2) on the up-current side was relatively larger, whereas the scour range of the other foundation piles (F_3 and F_4) was relatively small. With increases in the current velocity, the scour range expanded. The scour range for the F_1 and F_2 piles after 0.25 m/s of velocity action was approximately three times that after application of the 0.083 m/s velocity.

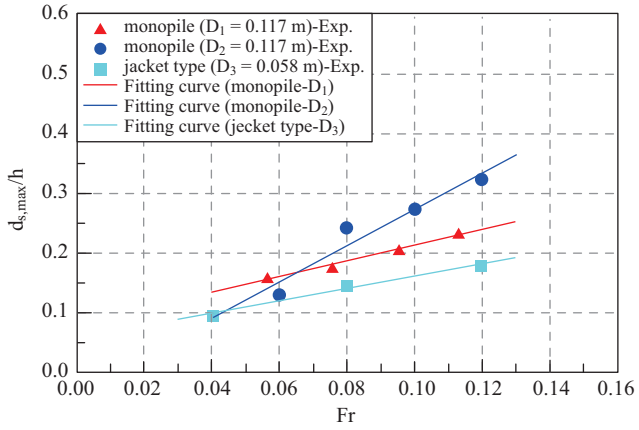

Fig. 9. The relationship between F_r and $d_{s,max}/h$ for the monopile and jacket-type foundations under different currents.

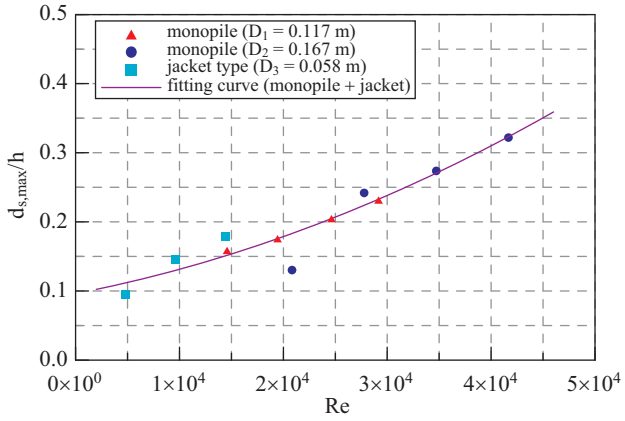

Fig. 11. The relationship between Re and $d_{s,max}/h$ for the monopile and jacket-type foundations under different currents.

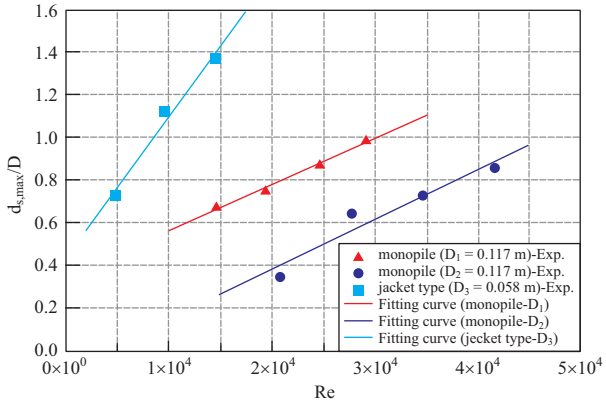

Fig. 10. The relationship between R_e and $d_{s,max}/D$ for the monopile and jacket-type foundations under different currents.

IV. MAXIMUM SCOUR DEPTH ANALYSIS

The dimensional analysis indicated that the maximum scour depth is related to relevant parameters. Thus, the dimensionless parameters of $d_{s,max}/D$ (or $d_{s,max}/h$) $\approx f(UD/\upsilon, U/\sqrt{gh})$ can be obtained through the π theorem, where UD/υ is the Reynolds number (R_e); $U/\sqrt{gh}$ is the Froude number (F_r); U is the current velocity; D is the diameter of the foundation; υ is the kinematic viscosity of the water; g is the gravity acceleration, and h is the water depth.

Fig. 9 and Fig. 10 show the maximum scour depth of the measurement of the monopile foundation with two different diameters and a jacket-type foundation diameter under different velocities. The relationships between the dimensionless maximum scour depth ($d_{s,max}/h$, $d_{s,max}/D$) corresponding to the Froude number (F_r) and Reynolds number (R_e) are plotted using a dimensional analysis. As shown in Fig. 9, the dimensionless maximum scour depth ($d_{s,max}/h$) of the monopile or jacket-type foundation is larger with increases in the Froude number (F_r). This indicates that for a greater current velocity at the same monopile foundation diameter and the same water depth, the maximum scour depth is also increased. In the case of the larger monopile foundation diameter under the same water depth and the same current velocity conditions, the maximum scour depth is also larger. Fig. 10 shows the relationship between the dimensionless maximum scour depth ($d_{s,max}/D$) and the corresponding Reynolds number (R_e). It can be clearly seen that under the same diameter foundation and the same water depth, the maximum scour depth of the monopile and the jacket-type foundation is significantly larger with increases in the Reynolds number (R_e). When there is a smaller pile diameter foundation, the increasing trend of the dimensionless maximum scour depth ($d_{s,max}/D$) is more obvious.

Furthermore, based on the comparison between Fig. 9 and Fig. 10, it was found that the variability of the dimensionless maximum scour depth increases with Reynolds number is much more obvious than the variability of the increase in the Froude number (F_r). The Fig. 11 shows the relationship between R_e and the maximum scour depth over water depth ($d_{s,max}/h$) for the monopile and jacket type foundations under different current levels. All the experimental data were used to estimate the possible maximum scour depth, and a fitting curve was obtained using a regression analysis. This regression curve can be used to estimate the maximum scour depth of a monopile foundation under different conditions in the future. Because the experimental studies of maximum scour depth are time-consuming and laborious, it is not possible to obtain complete data at the moment, and the test conditions will be added in the future. More complete and specific results will be analyzed to provide a reference for engineering applications.

V. CONCLUSION

In this study, hydraulic model experiments were performed under various current velocities, and relevant parameters were applied to explore and compare the maximum scour depth and the potential scour area around monopile and jacket-type foundations of various diameters. The experimental results indicated

that the maximum scour depth initially occurred on the up-current side of the monopile, and a semicircular scour hole gradually developed on the up-current side of the monopile. Simultaneously, a conical scour hole formed on the down-current side of the monopile, and a deposition phenomenon on the down-streaming side of the scour hole was observed. In all of the experiments, the relationships between the dimensionless maximum scour depth and the corresponding test duration were plotted to observe the scour depth development around the structure foundations. Furthermore, the relationships between the dimensionless maximum scour depth and the corresponding Froude number (F_r) and Reynolds number (R_e) were plotted through the use of a dimensional analysis. It was found that the increase in the variability of the dimensionless maximum scour depth with Reynolds number was more obvious than the variability of the increase in the Froude number. The relationship between the Reynolds number (R_e) and the relative scour water depth ($d_{s,max}/h$) can be obtained as a regression curve. This fitting curve provides a simple way to estimate the maximum scour depth around a monopile foundation under different current speeds (U), water depths (h) and pile diameters (D). However, more complete and specific results will be analyzed to provide a reference of engineering applications in the future.

REFERENCES

Breusers, H. N. C., G. Nicollet and H. W. Shen (1977). Local scour around cylindrical piers. Journal Hydraulic Research 15, 211-252.

Chen, H. H., R. Y. Yang and H. H. Hwung (2014). Study of hard and soft countermeasures for scour protection of the jacket-type offshore wind Turbine Foundation. Journal of Marine Science and Engineering (JMSE) 2(3), 551-567.

Dean, R. G. and R. A. Dalrymple (1985). Water Wave Mechanics for Engineering and Scientists. World Scientific, Singapore.

den Boon, J. H., J. Sutherland, R. Whitehouse, R. Soulsby, C. J. M. Stam, K. Verhoeven, M. Høgedal and T. Hald (2004). Scour Behaviour and Scour Protection for Monopile Foundations of Offshore Wind Turbines, ResearchGate, https://www.researchgate.net/publication/228691951.

Hotta, S. and N. Marui (1976). Local Scour Amd Current Around a Porous Breakwater. Proceedings of 15th Conference on Coastal Engineering, Honolulu, Hawaii, USA, 1590-1604.

Oumeraci, H. (1984). Scale effects in coastal hydraulic models. Symp. In Scale effects in modelling hydraulic structures, 7(10), 1-7, Edited by: Kobus, H. Esslingen: Technische Akademie.

Raudkivi, A. J. and R. Ettema (1983). Clear-Water Scour at Cylindrical Piers. Journal of Hydraulic Engineering, ASCE 109(3), 338-350.

Stahlmann, A. and T. Schlurmann (2012). Numerical and Experimental Modeling of Scour at Tripod Foundations for Offshore Wind Turbines, 6th International Conference on Scour and Erosion, ICSE-6, Paris.

Sumer, B. M., J. Fredsøe and N. Christiansen (1992). Scour around vertical pile in waves. Journal of Waterway, Port, Coastal, and Ocean Engineering, ASCE, Vol. 118, No. 1, 15-31.

Sumer, B. M., N. Christiansen and J. Fredsøe (1993). Influence of cross-section on wave scour around piles. Journal of Waterway, Port, Coastal, and Ocean Engineering, ASCE 119(5), 477-495.

Zhao, M., Cheng, L. and Z. Zang (2010). Experimental and numerical investigation of local scour around a submerged vertical circular cylinder in steady currents, Coastal Engineering 57, 709-721.